

AD-A077 110

TECHNICAL LIBRARY

AD

AD-E400 364

TECHNICAL REPORT ARLCD-TR-79033

OPTICAL EXTINCTION AND N_2 GAS EVOLUTION ON PHOTODECOMPOSITION OF $Pb(N_3)_2$

WAYNE GARRETT
DONALD A. WIEGAND

SEPTEMBER 1979



US ARMY ARMAMENT RESEARCH AND DEVELOPMENT COMMAND
LARGE CALIBER
WEAPON SYSTEMS LABORATORY
DOVER, NEW JERSEY

APPROVED FOR PUBLIC RELEASE; DISTRIBUTION UNLIMITED.

The views, opinions, and/or findings contained in this report are those of the author(s) and should not be construed as an official Department of the Army position, policy or decision, unless so designated by other documentation.

Destroy this report when no longer needed. Do not return it to the originator.

UNCLASSIFIED

SECURITY CLASSIFICATION OF THIS PAGE (When Data Entered)

| REPORT DOCUMENTATION PAGE | | READ INSTRUCTIONS BEFORE COMPLETING FORM |
|--|-----------------------|--|
| 1. REPORT NUMBER Technical Report ARLCD-TR-79033 | 2. GOVT ACCESSION NO. | 3. RECIPIENT'S CATALOG NUMBER |
| 4. TITLE (and Subtitle) OPTICAL EXTINCTION AND N ₂ GAS EVOLUTION ON PHOTODECOMPOSITION OF Pb(N ₃) ₂ | | 5. TYPE OF REPORT & PERIOD COVERED Final 1972-1975 |
| | | 6. PERFORMING ORG. REPORT NUMBER |
| 7. AUTHOR(s) Wayne Garrett and Donald A. Wiegand | | 8. CONTRACT OR GRANT NUMBER(s) |
| 9. PERFORMING ORGANIZATION NAME AND ADDRESS Energetic Materials Division Large Caliber Weapon Systems Laboratory US ARMY, ARRADCOM, Dover, NJ 07801 | | 10. PROGRAM ELEMENT, PROJECT, TASK AREA & WORK UNIT NUMBERS |
| 11. CONTROLLING OFFICE NAME AND ADDRESS US Army Armament Research and Development Command ATTN: DRDAR-TSS Dover, NJ 07801 | | 12. REPORT DATE September 1979 |
| | | 13. NUMBER OF PAGES 41 |
| 14. MONITORING AGENCY NAME & ADDRESS (if different from Controlling Office) US Army Armament Research and Development Command ATTN: DRDAR-LCE Dover, NJ 07801 | | 15. SECURITY CLASS. (of this report) UNCLASSIFIED |
| | | 15a. DECLASSIFICATION/DOWNGRADING SCHEDULE |
| 16. DISTRIBUTION STATEMENT (of this Report) Approved for public release, distribution unlimited. | | |
| 17. DISTRIBUTION STATEMENT (of the abstract entered in Block 20, if different from Report) | | |
| 18. SUPPLEMENTARY NOTES | | |
| 19. KEY WORDS (Continue on reverse side if necessary and identify by block number) Lead azide Photodecomposition Colloidal disorder optical bleaching Index of refraction of lead azide | | |
| 20. ABSTRACT (Continue on reverse side if necessary and identify by block number) The slow decomposition of lead azide single crystals was studied by measurement of changes in optical extinction and N ₂ gas evolution due to visible, ultraviolet, and x-ray irradiation. Direct comparisons of total N ₂ evolved and changes in optical density as a function of irradiation time for a given sample allow a simple interpretation of the decomposition processes in terms of simultaneous colloidal lead and N ₂ formation. Kinetic studies, as a function of wavelength and intensity, further indicate that the rate of decomposition is simply related to the rate of energy absorption and the amount of decomposition. | | |

UNCLASSIFIED

SECURITY CLASSIFICATION OF THIS PAGE(When Data Entered)

BLOCK 20: ABSTRACT Cont'd

For weakly absorbed radiation, a monomolecular decomposition process is indicated. The colloidal Pb was found to be, in some cases, highly reactive with air and evidence for Pb metal production was found for irradiation in high vacuum. Evidence for N₂ trapping was also observed. Decomposition efficiencies were studied as a function of wavelength and temperature; the thermal stability of the disorder was investigated; and optical bleaching effects were observed. Polarized light measurements of the optical extinction indicate that it is primarily due to absorption by Pb colloids.

UNCLASSIFIED

SECURITY CLASSIFICATION OF THIS PAGE(When Data Entered)

TABLE OF CONTENTS

| | Page No. |
|--|----------|
| Introduction | 1 |
| Experimental | 2 |
| Results | 3 |
| Kinetics | 3 |
| N ₂ Evolution Versus Colloidal Pb Formation | 10 |
| Stability of Irradiation Induced Disorder and Surface Reactions | 10 |
| Efficiency of N ₂ Evolution | 13 |
| Optical Bleaching | 15 |
| Colloidal Lead and Lead Metal Production | 18 |
| Index of Refraction Measurements | 20 |
| Optical Extinction Studies Using Polarized Light | 21 |
| Discussion | 24 |
| Structure and Surface Morphology of Irradiated Lead Azide | 24 |
| Decomposition Model | 26 |
| References | 31 |
| Distribution List | 35 |

FIGURES

| | Page No. |
|---|----------|
| 1. Quantum efficiency for N ₂ gas evolution versus time of irradiation as a function of wavelength (and intensity for 365 nm irradiation) as measured in the high vacuum system. For clarity, the 365 nm exposure at reduced intensity is plotted on a separate scale. | 5 |
| 2. Change in optical density at 410 nm versus UV irradiation time. Irradiation and measurement at indicated temperatures in the vacuum cryostat. | 6 |
| 3. Change in optical density at 410 nm versus x-ray irradiation time. Irradiation and measurement at 78K and 300K in the vacuum cryostat. | 8 |
| 4. Change in optical density per hour measured at 420 nm versus irradiation intensity at 435.9 nm. Sample at room temperature in the vacuum cryostat. | 9 |
| 5. Change in optical density at 420 nm versus total nitrogen evolved and measured in the high vacuum system. Only qualitative features of the curves at 80K and 300K should be compared since the experimental conditions were different for the two temperatures. | 11 |
| 6. Dependence of quantum efficiency on wavelength for nitrogen evolution as measured in the high vacuum system at room temperature. Shown also for comparison is the optical density of a thin film as measured by Fair and Forsyth (ref. 13) at low temperature. | 14 |
| 7. Decrease in optical density versus wavelength due to exposure to 546 nm radiation. Sample previously UV-irradiated. All irradiation and measurements at room temperature in the vacuum cryostat. | 16 |
| 8. <u>Decrease</u> in optical density versus wavelength, λ , due to exposure to air of a sample previously UV irradiated in high vacuum, Scale B. Also shown is the curve of <u>increase</u> of optical density versus λ due to UV irradiation with sample in high vacuum, Scale A. | 17 |

9. Increase in optical density versus λ due to irradiation with 435.6 nm light. Data is given for the electric field, \vec{E} , parallel to the \vec{b} (Curve A) and \vec{c} (Curve B) crystallographic directions.

INTRODUCTION

The photodecomposition of lead azide powders (refs. 1,2), crystals (refs. 3,4,5) and thin films (refs. 6,7) has previously been studied by monitoring the nitrogen gas resulting from irradiation. Recently, the decomposition of single crystals was studied for the first time by monitoring the change in optical extinction resulting from the formation of colloidal lead, the other end product of decomposition (ref. 8).

Several theories have been proposed to explain how the initial photon flux is converted to the observed end products (refs. 7,9,10,11). These theories generally involve electronic transitions that form neutral azide molecules, i.e.,



which may react to form nitrogen:



with electrons being captured by the metallic nuclei, i.e.,



Intermediate reaction steps involving diffusion of the observed end products are not considered in a description of the decomposition process because properties such as diffusion constants, intrinsic lattice disorder, etc., are not known for this material. Further, the correlation of the rates of decomposition of the azide and lead sublattices as suggested by Reactions (1) and (2) has always been assumed but not demonstrated experimentally. Catalytic effects on the nitrogen rate due to the presence of metallic nuclei have been considered to explain kinetic results in other azides (ref. 11).

To aid in formulating a more complete decomposition model, we have made simultaneous measurements of the kinetics of decomposition of both the lead and the azide sublattices under varying experimental conditions of exciting wavelength and sample temperature. For these studies, polished single crystal plates were required not only for optical measurements but also to minimize surface to volume problems inherent in powder samples. In addition, an ultra-high vacuum system was used in several cases so that fractional monolayers of gas evolution could be detected and surface reactions could be minimized.

EXPERIMENTAL

Single crystal samples of $\text{Pb}(\text{N}_3)_2$ for photodecomposition measurements were grown from a 20% aqueous solution of ammonium acetate by slow cooling (ref. 12). Crystal plates, approximately $4 \times 4 \times 1$ mm, were cut from large crystals and polished to obtain a minimum optical density (O.D.) of ~ 0.1 due to surface scattering and reflection.

The vacuum decomposition apparatus allowed for simultaneous measurements of gas evolution rates and changes in the optical density as a function of wavelength. The ion-pumped high vacuum system reached a base pressure of approximately 1×10^{-8} torr with either a low temperature bake, (below 100°C), or without baking. Gas pressure was detected with either a Bayer-Alpurt gauge or a Residual Gas Analyzer (RGA), and the rate was measured directly by pumping on the 2-liter sample chamber through a partially opened valve. With this arrangement, a minimum rate of approximately 10^{11} molecules/sec was detectable.

Samples were irradiated using a high-pressure Hg lamp with filters to isolate spectral lines. A maximum intensity of approximately 10^{15} photons/cm²-sec was obtained with the 365 nm filter. For the spectral dependence of the gas evolution rate, a Gaertner quartz prism monochromator was used with a 1000 watt Xe-Hg source.

Measurements of the changes in optical density (Δ O.D.) as a function of wavelength were made in the high vacuum system using a tungsten lamp in conjunction with a double monochromator consisting of a Perkin-Elmer prism monochromator, Model 98, and a Bauch and Lomb f/3.5 grating monochromator, Model 33-86-25, in tandem. The exit slit of the Bauch and Lomb monochromator was focused by a quartz lens through a sapphire window onto the sample and the transmitted beam detected through a second sapphire window by an S-20 response photomultiplier. Stray light limited the maximum O.D. obtainable to about 4.0, but only O.D.'s lower than 2.0 were actually used in the data analyses. An initial scan of wavelengths from 800 nm to the high absorption edge was made to determine I_0 , the transmitted intensity before decomposition. The Δ O.D. was calculated from:

$$\Delta \text{ O.D. } (t) = \log \frac{I_0(\lambda)}{I(\lambda, t)}$$

where $I(\lambda, t)$ is the intensity transmitted after decomposition for time t . During the decomposition run, I_0 was monitored intermittently with time by deflecting the incident beam with a mirror onto a silicon probe used with a Cintra Model 101 radiometer. Absolute light intensities, for the calculation of efficiencies, were measured using the same radiometer and sensor which was, in turn, calibrated against a standard lamp.

The crystal was mounted with epoxy to a sapphire disk for room temperature (RT) measurements in the high vacuum system. At liquid nitrogen temperature (LNT), in the same system, the crystal was glued directly with silver paint to a copper block that was in mechanical contact with the cold finger. This copper block was surrounded by a thermal shield with holes for a light path. Warming from LNT was accomplished by blowing hot air (200°C) into the cold finger. A platinum resistor mounted next to the sample with silver paint was used for temperature monitoring.

Optical measurements were also made using a Cary 14 R spectrophotometer with the sample mounted in a metal vacuum cryostat (ref. 8). The wavelength range between 2500 nm and the edge for high absorption (~ 400 nm) was investigated. Optical densities up to 5.0 could be measured. The pressure at the pumps was $\sim 10^{-6}$ torr in most cases, but the pressure in the cryostat at the sample position was higher. An oil diffusion pump and liquid nitrogen cold trap were used. The optical density as recorded by the Cary 14 R was the same as that measured in the high vacuum described above. The same high pressure Hg lamp in conjunction with band pass and interference filters were used with this system for producing decomposition. In addition, an x-ray source (Machlett tube) operating at 50kV, 40 ma with a W anode was used. The sample to anode distance was of the order of 2 inches and the x-rays were filtered by an Al window 0.1 mm thick plus the Be window of the x-ray tube. A He-Ne laser was also used to obtain 628 nm radiation. In addition, it was necessary to use a lens to focus this radiation to obtain measurable changes in the optical density.

RESULTS

Kinetics

The rate of nitrogen evolution and the rate of colloidal metal formation as detected by changes in the optical density were measured as a function of wavelength, intensity and sample temperature. The quantum efficiency, η , [$\eta = (dN_2/dt)/(\text{Photons/sec})$] for nitrogen release is plotted in figure 1, for irradiation with three UV narrow band pass filters. As the photon flux is a constant for any one wavelength, the curves in figure 1 are essentially a plot of the rate of nitrogen evolution vs. time. The rate of nitrogen evolution for these strongly absorbed wavelengths exhibits an "induction period," where the rate remains constant or increases only slowly with time, an acceleration to a maximum, followed by decay to a nearly constant rate for long time periods. It should be noted that the rate decay is more pronounced when plotted on a linear scale. These characteristics of the rate curve, excluding the induction period, were previously observed

on powders using 253 nm light (ref. 1), and the induction period was observed on powders using longer wavelength (405 nm) radiation (ref. 5).

The induction period is seen most pronounced in figure 1 with 365 nm light at reduced intensity. It is observed on the first irradiation of an unirradiated crystal or on a crystal on which the surface damage has been removed by polishing. Approximately 2% of the nitrogen is removed within a distance $1/\alpha$ from the surface, where α is the absorption coefficient. Once it occurs, however, the induction period is not observed on reirradiation unless the sample is annealed by a low temperature bake ($\sim 75^\circ\text{C}$) for several hours or allowed to remain at room temperature for a minimum of 3 days. A longer annealing time restores a greater percentage of the original induction period time.

The induction period is also affected by changes in light intensity and wavelength. The amount of gas released during the induction period,

i.e., $\int \frac{dN_2}{dt} dt$, varies nearly linearly with light intensity at any

particular UV wavelength. Thus, reduced intensities expand the rate curve time-wise as can be seen in figure 1 for the 365 nm case. The UV wavelengths having larger absorption coefficients produce more nitrogen molecules per photon; and so behave in a manner similar to light of higher intensity. The net effect is to increase the rate and reduce the time scale as seen in figure 1 for the 313 nm irradiation. The complete spectral dependence over the wavelength region from 300 to 400 nm is discussed in a subsequent section.

At LNT both the rate of nitrogen release and the rate of colloid formation are reduced. This effect is shown for the case of colloid formation in figure 2; and a linear relationship is shown below to exist between the rates of colloid formation and gas evolution following the induction period. During the induction period the rate reduction factor at LNT is approximately 100, whereas at the maximum rate, the reduction is only about 5.

These properties of the induction period, together with results from other decomposition studies, suggest the trapping of nitrogen gas in the crystal lattice. The presence of trapped nitrogen was confirmed in the present study by observing bubbles escaping during slow dissolution in dilute nitric acid (0.01 M). The bubbles, observed microscopically, come only from the irradiated region of a crystal and are observable with even the small doses required to complete the induction period. The presence of trapped nitrogen has also been observed in thin films (ref. 6), although no induction period is observed for films.

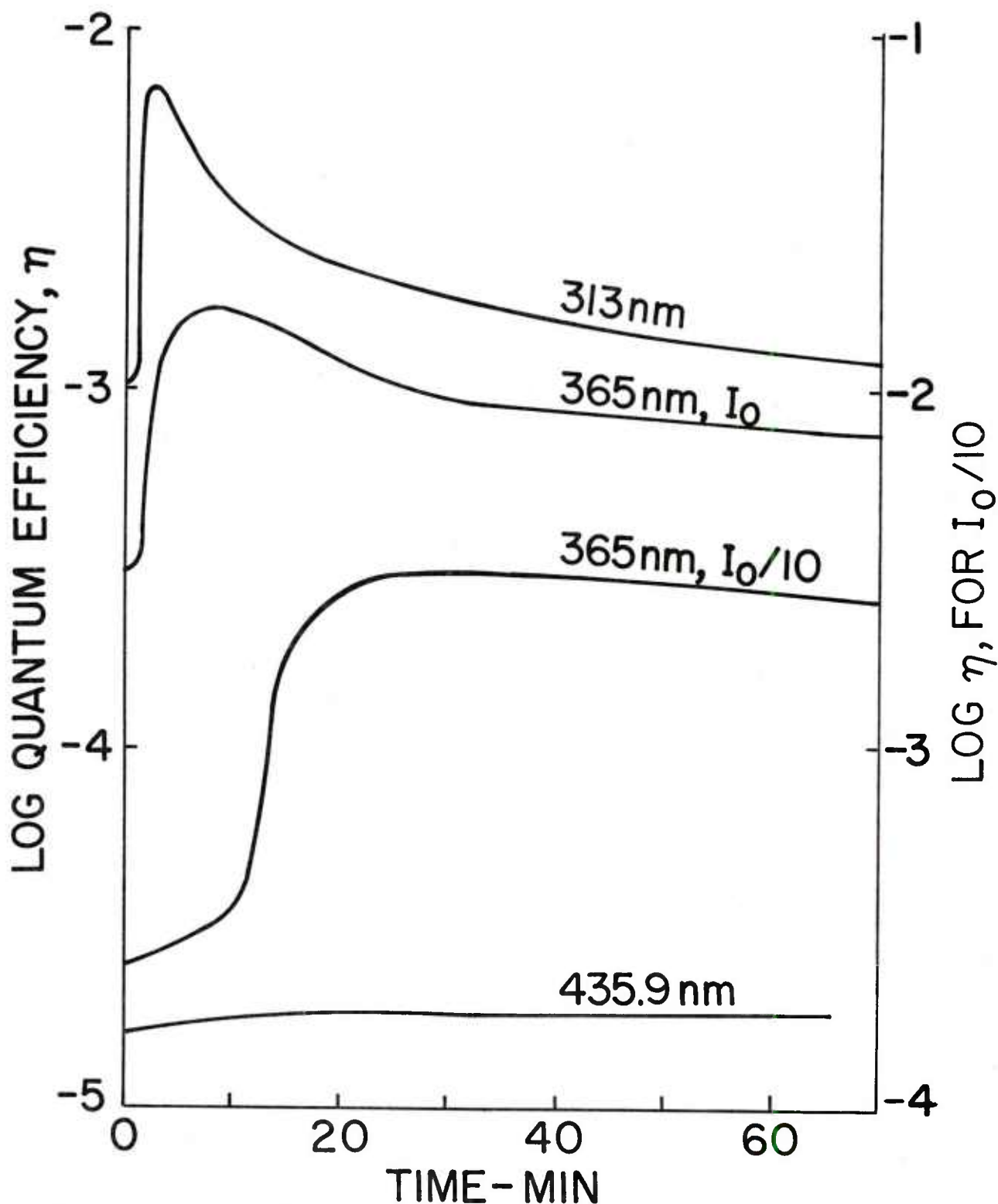


Figure 1. Quantum efficiency for N_2 gas evolution versus time of irradiation as a function of wavelength (and intensity for 365 nm irradiation) as measured in the high vacuum system. For clarity, the 365 nm exposure at reduced intensity is plotted on a separate scale.

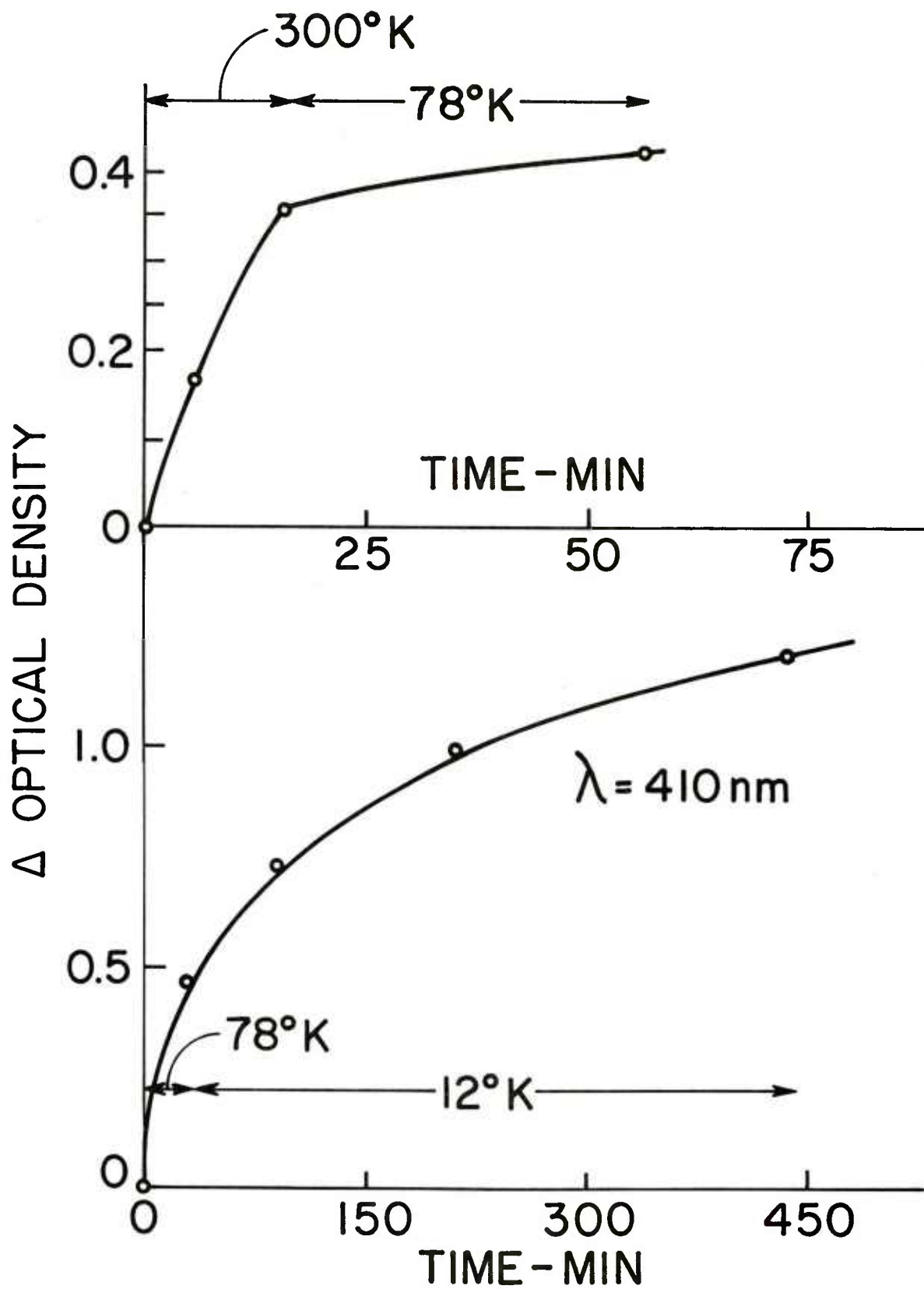


Figure 2. Change in optical density at 410 nm versus UV irradiation time. Irradiation and measurement at indicated temperatures in the vacuum cryostat.

The colloidal Pb formation, as determined by O.D. changes, is shown in figure 2, for UV exposure and measurement at the temperatures indicated. This figure shows a growth to saturation occurring even at 12K (ref. 8). The relationship between the total N₂ evolved and the amount of colloidal Pb detected by optical measurements is discussed below.

The data of figure 2 indicate a decrease in the rate of colloidal Pb formation by approximately a factor of 10 on cooling from 300K to 78K. Other data indicate that the rate of colloidal Pb formation is decreased on cooling much more in the initial stages of irradiation than in the later stages. Thus, for UV irradiation both the rate of nitrogen evolution and the rate of colloidal metal formation decrease in the same general manner on reduction of temperature. The data of figure 2 do not indicate a significant further reduction in the rate of colloid formation on decreasing the temperature from 78 to 12K. More quantitative comparison of N₂ evolved and colloidal Pb produced are discussed below.

Decomposition was also studied using more penetrating x-rays and weakly absorbed light at 435, 545, 578, and 630 nm. In figure 3 the change in optical density is displayed as a function of time of x-ray exposure at 300 and 78K. This linear growth, which also is observed for all of the above wavelengths, is in sharp contrast to the saturation results found for UV irradiation. Thus, all of the wavelengths used for irradiation, except those in the high absorption coefficient range, give linear Δ O.D. vs. time curves. It is also to be noted that the efficiency of formation of colloidal metal for x-ray exposure is relatively insensitive to temperature, in sharp contrast to the strong temperature dependence for UV irradiation (fig. 2).

The gas evolution rates for irradiation using a 435 nm narrow band pass filter was constant for several hours of exposure (fig. 1). Because of the small absorption coefficient for this wavelength, the gas evolution rates are small ($\sim 10^{10} \frac{\text{molecules}}{\text{cm}^2 - \text{sec}}$) and significant amounts of nitrogen are probably trapped in the crystal; however, there is agreement in that the decomposition rates of both the lead and azide sublattices are linear for this weakly absorbed wavelength.

In figure 4, the slopes of curves such as that of figure 3, i.e., $\Delta \text{O.D.} / \text{time}$, is given vs. light intensity for $\lambda = 435$ radiation at 300K. The linear dependence on intensity suggests the possibility of very simple kinetics of decomposition for weakly absorbed light (and therefore low energy absorbed per unit volume). Unfortunately, it was not possible to make measurements of gas evolution as a function of intensity because of lack of sensitivity.

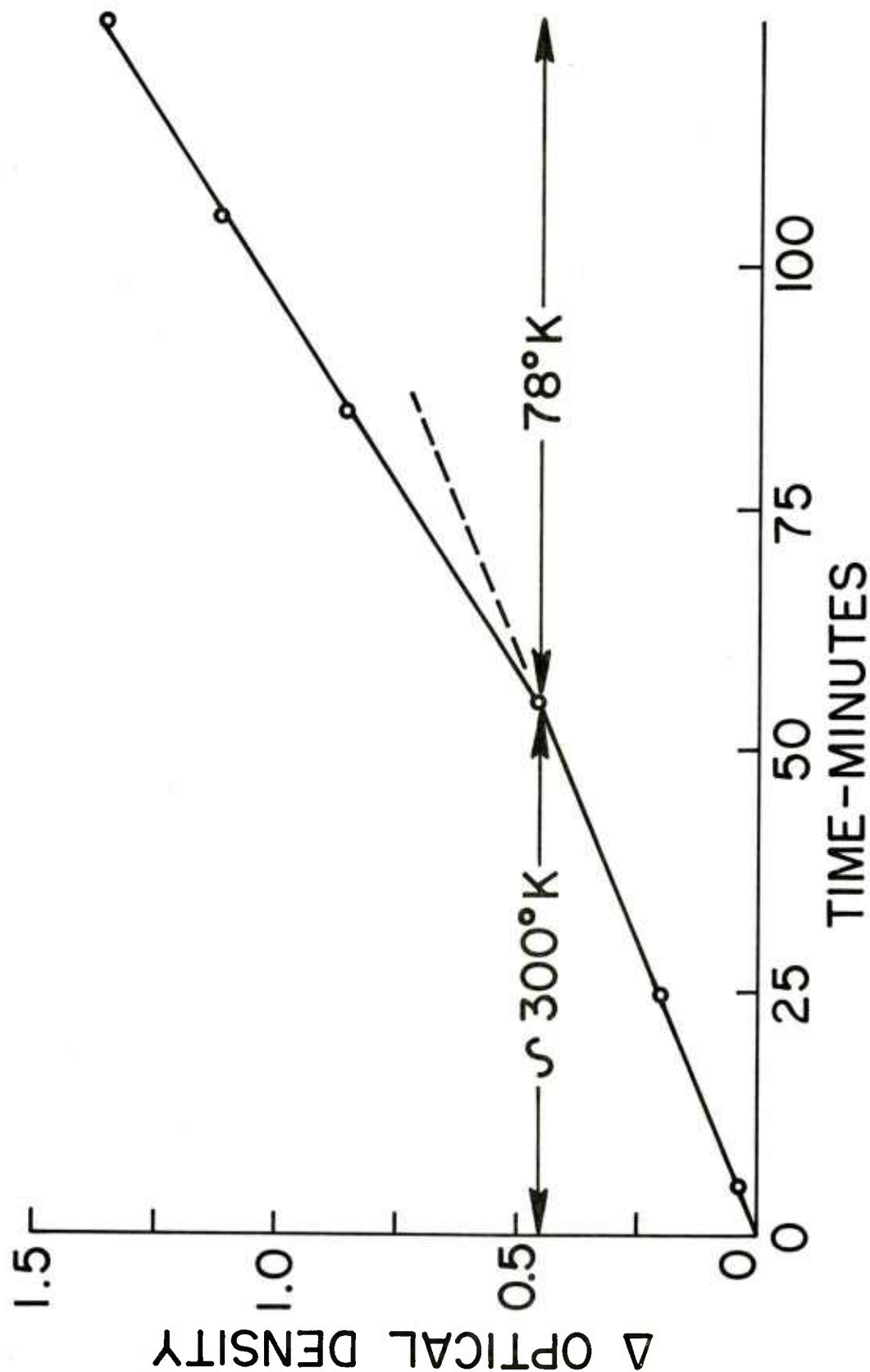


Figure 3. Change in optical density at 410 nm versus x-ray irradiation time. Irradiation and measurement at 78K and 300K in the vacuum cryostat.

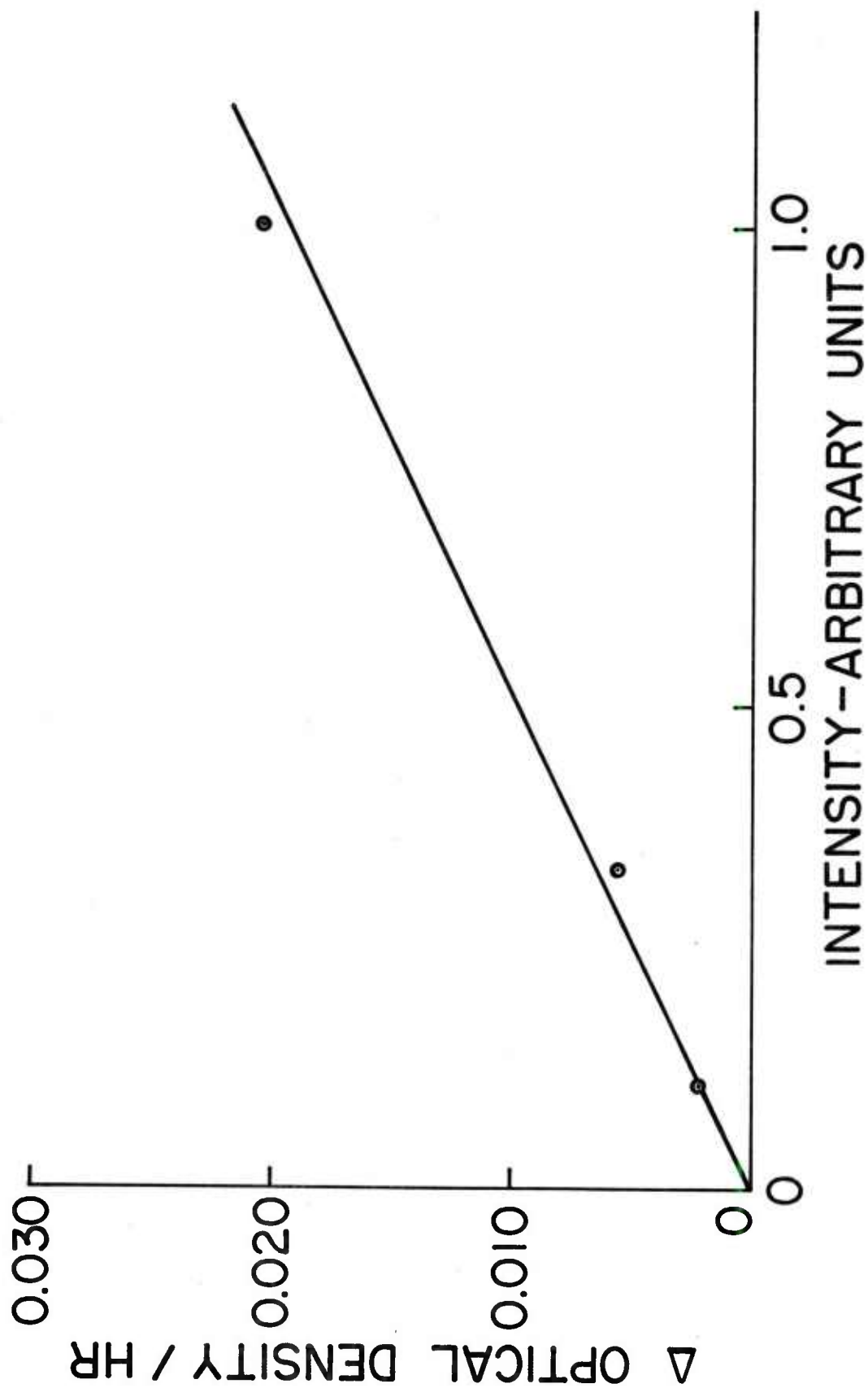


Figure 4. Change in optical density per hour measured at 420 nm versus irradiation intensity at 435.9 nm. Sample at room temperature in the vacuum cryostat.

N₂ Evolution Versus Colloidal Pb Formation

In order to make a more direct comparison between the decomposition of the lead and azide sublattices than the kinetic data alone allows, both gas evolution rates and optical extinction measurements were made in situ in the high vacuum system. Figure 5 plots the change in optical density at 420 nm (double monochromator arrangement) vs. the corresponding amount of N₂ released for exposure at 365 nm (narrow band pass filter) both at RT and at LNT.

Several features of the curves (fig. 5) provide information concerning the nature of the decomposition process. First, the rate of colloidal lead formation increases in the initial stages (induction period, fig. 1) faster than the N₂ evolution. This result supports the hypothesis that N₂ is being trapped in the lattice in this stage. Following the induction stage, there is a linear relationship between Pb colloid formation and N₂ evolution at RT and LNT up to an O.D. change of about 1.0 (corresponding to approximately 30% N₂ removed within a distance $1/\alpha$ from the surface at 300K). This indicates simultaneous decomposition of the lead and azide sublattices.

The saturation at higher O.D.'s at RT may be a consequence of one or more of several effects. Calculations have shown that surface colloids, being surrounded by a medium of lower refractive index, contribute less to the total extinction (by a factor of about 10) than do bulk colloids surrounded by Pb(N₃)₂ (ref. 8) (see also DISCUSSION section).

Stability of Irradiation Induced Disorder and Surface Reactions

The optical extinction due to irradiation of Pb(N₃)₂ has been found to be at least partially unstable under some conditions. If a sample is exposed to ultra-violet light at room temperature in the high vacuum system the increased optical density in the visible range is stable if the high vacuum is maintained and the sample kept in the dark. However, on exposure to air the optical density decreases by 20 to 40%. The wavelength dependence of the optical density after exposure to air has approximately the same form as that produced on irradiation, indicating the decrease is primarily due to decreased extinction of colloidal lead. However, a "flattening" of the optical density curve at longer wavelengths suggests the decreased extinction is partly associated with the presence of at least a small amount of lead metal (relative to the amount of colloidal lead). The relationship between lead metal and colloidal metal is discussed below. The changes are small and additional experiments are necessary to verify this conclusion.

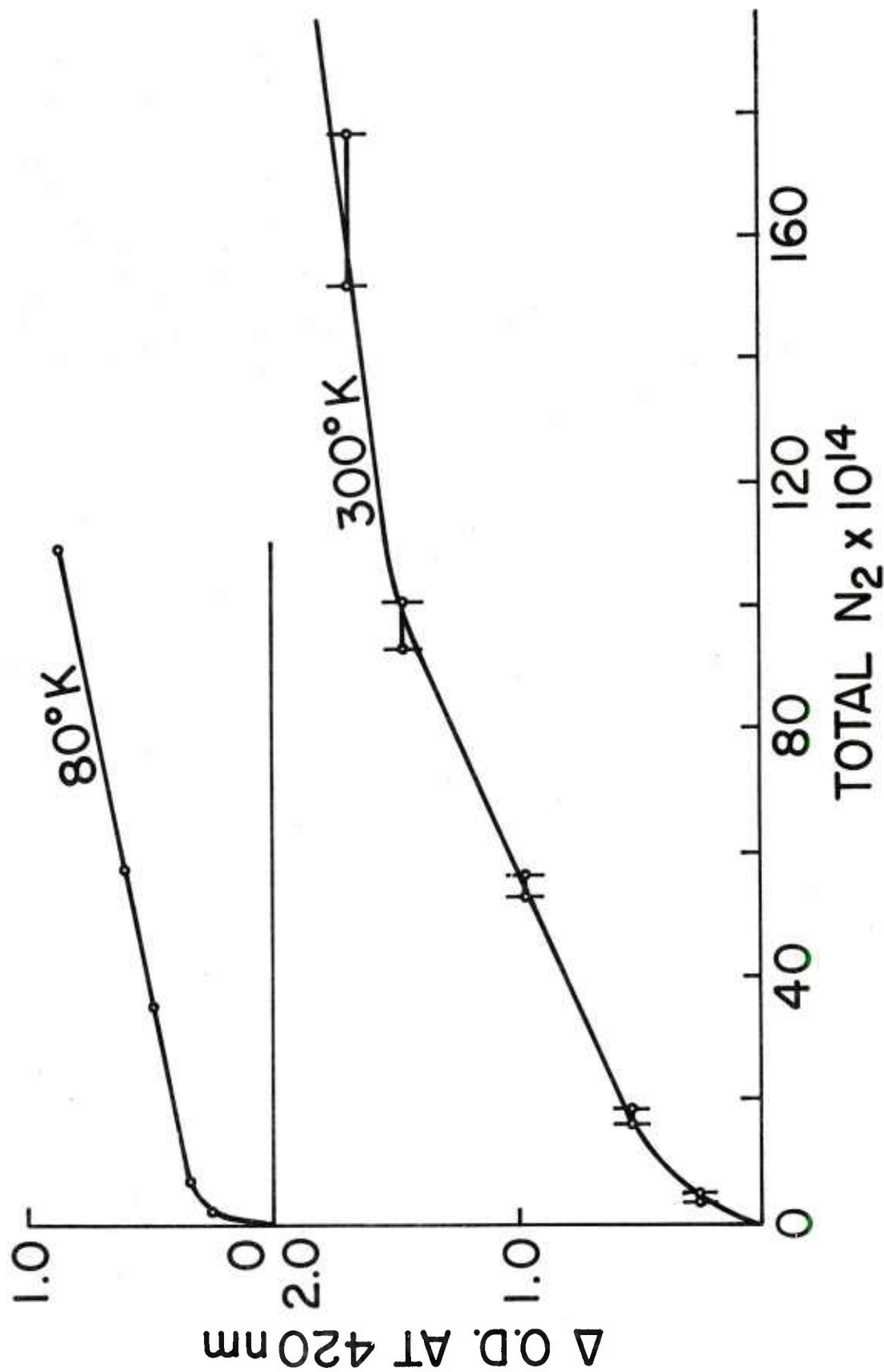


Figure 5. Change in optical density at 420 nm versus total nitrogen evolved and measured in the high vacuum system. Only qualitative features of the curves at 80K and 300K should be compared since the experimental conditions were different for the two temperatures.

In general, the percentage decrease in optical density on pressure rise in either the high vacuum system or the cryostat was larger when the sample was exposed while at 80K than when exposed at 300K. A sample UV irradiated in the high vacuum system at approximately 80K exhibited no decrease in the irradiation induced optical density on warming to room temperature. However, the optical density decreased significantly ($\sim 60\%$) when air was admitted to the system. In contrast, some samples exposed to UV or x-ray irradiation while in the vacuum cryostat at 80K showed significant decreases in low temperature-induced optical density on warming and in some cases all of this irradiation-induced optical density "annealed" on warming to room temperature. In all cases where this thermal "annealing" occurred, there was also a significant pressure rise in the system in the same temperature range due to gases escaping from the inner walls of the cryostat. The temperature range of "annealing" and pressure rise varied from run to run. For one sample there was not a significant pressure rise during warming and the optical density did not decrease. The optical density did however, decrease slowly at a decreasing rate over a period of several days at room temperature. Additional decreases were observed on warming above room temperature, but the optical density observed on first cooling to room temperature was stable over a period of several days. While the pressure at the sample in the cryostat is unknown, the pressure at the pump was 3×10^{-6} torr. The cryostat was connected to the pump by four feet of flexible metal hose, one inch in diameter. These results are discussed below.

Attempts were subsequently made to determine if nitrogen gas was also evolved on warming. There are several reports in the literature that gas release does occur from powders of lead azide after exposure at low temperatures (ref. 2,10). Single crystal samples mounted in the high vacuum system in good thermal contact with a copper cold finger at LNT, were exposed for approximately 20 minutes to the Hg lamp through a Corning 7-60 filter that passes light in a broad band of wavelengths from 300 to 400 nm. Following irradiation, the crystals were warmed to 350K in the dark. Thermal gas evolution peaks were observed using a RGA detector on samples cycled to low temperature and warmed with and without irradiation at low temperature. Although several desorption peaks were detected, only one peak, predominately N_2 , at 150K was found to occur for all irradiated samples. The amount of N_2 released during warming at 150K was of the order of one monolayer of nitrogen on the surface of the crystal. It was assumed that this represented physically adsorbed nitrogen. This amount is approximately 1/100th of the nitrogen evolved on irradiation at LNT before warming. Simultaneous monitoring of the crystal O.D. on warming from LNT in the high vacuum system failed to show any changes in O.D. even at 150K.

Efficiency of N_2 Evolution

The spectral dependence of the nitrogen evolution rate was determined at discrete wavelengths with the Gaertner monochromator over the range from 300-380 nm in the high vacuum system. To minimize the total exposure, and thus the amount of decomposition during this series of exposures, the initial rate due to light exposure, i.e., $dN_2(\lambda)/dt$ as $t \rightarrow 0$ was measured. Separate experiments showed that dN_2/dt as $t \rightarrow 0$ was related through a constant to the maximum gas evolution rate (the maximum in the quantum efficiency in fig. 1). All samples were exposed sufficiently to eliminate the induction period before measuring these rates. Light intensities were determined with the Cintra Radiometer.

The results of these measurements along with a plot of the optical density of a lead azide thin film (ref. 13) is shown in figure 6. This efficiency curve which is a plot of the maximum gas evolution rate calculated from the measured initial rate and normalized to light intensity is also similar to that observed for the gas evolution efficiency of thin films (ref. 6). The fact that all photons are absorbed by the crystal in this wavelength region (absorption coefficients are greater than 10^{-4}) indicates that the efficiency also depends on the diffusion of nitrogen to the surface. The intensity dependence of the maximum rate at any one wavelength in the range from 300 to 400 nm was found to be sublinear i.e., the rate as defined above varies as $I^k(\lambda)$, where k varied for those wavelengths examined between $1/3$ and $2/3$. For the case of thin films, as measured by Hall (ref. 6), k varied from $1/3$ at low intensities to $3/2$ for the highest intensity. Many of the results on thin films are in general agreement with those on crystals since it has been demonstrated that changes in wavelength or intensity produce similar changes in the rate curves. Measurements made on powders at 253 nm show a linear dependence (ref. 2). Intensity dependences have generally been used to predict the order of the decomposition kinetics and so the possible reaction steps (ref. 11). For the intensities used in this study, the higher rates observed for greater photon flux densities are not the result of a superlinear intensity dependence. These results suggest that the decomposition must be occurring in the region of absorption, as suggested by Williams et al. (ref. 7), so that the rate depends on the energy absorbed per unit volume. In addition, the rate may also depend on the diffusion of nitrogen to the surface, so that shorter wavelength radiation produces a larger concentration of nitrogen near the surface giving rise to a higher efficiency.

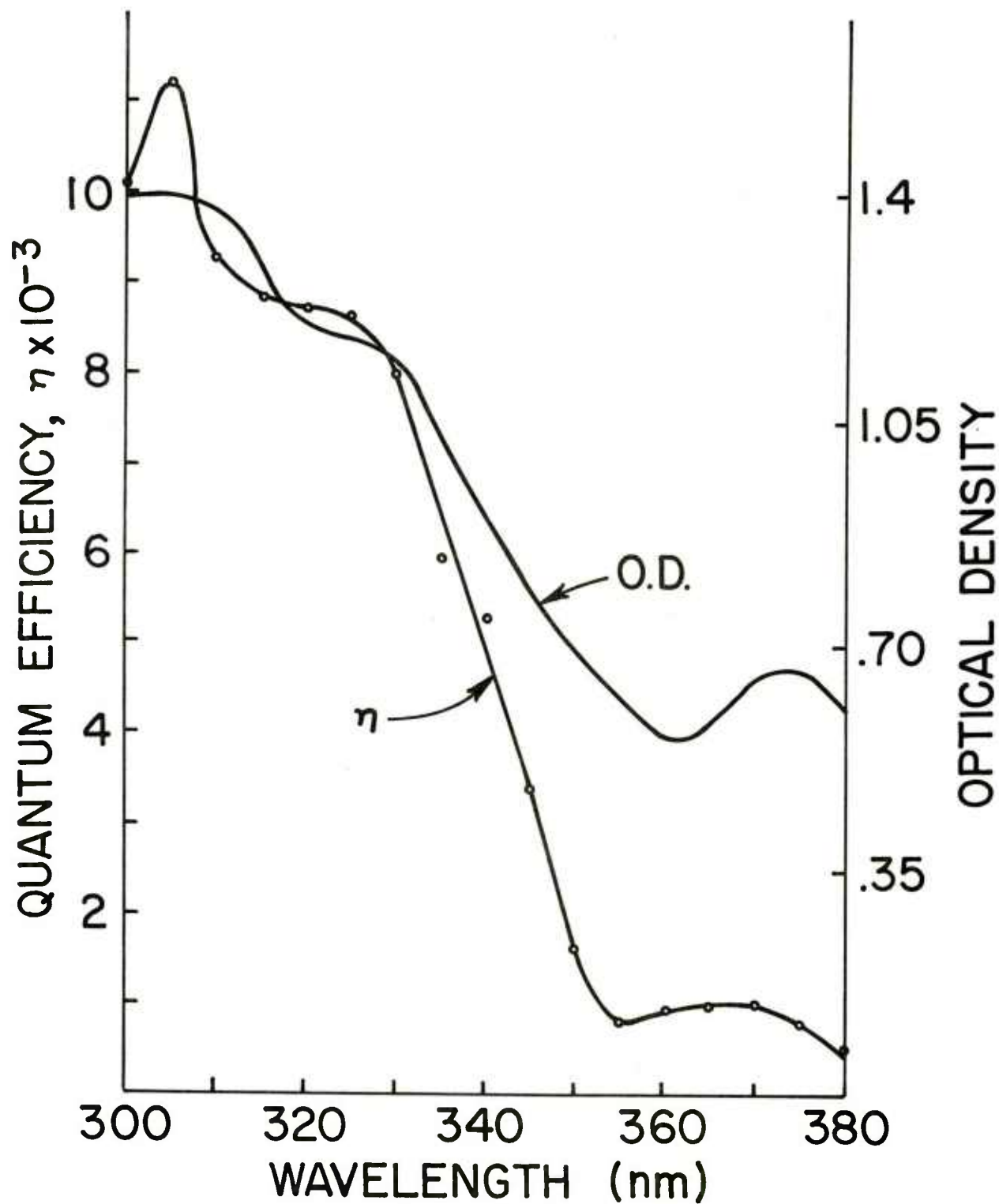


Figure 6. Dependence of quantum efficiency on wavelength for nitrogen evolution as measured in the high vacuum system at room temperature. Shown also for comparison is the optical density of a thin film as measured by Fair and Forsyth (ref. 13) at low temperature.

Optical Bleaching

When a previously unirradiated sample is exposed to light with $\lambda > 405$ nm, the optical density increases and has the characteristic wavelength dependence expected of colloidal Pb disorder, as discussed above. However, a sample previously exposed to ultraviolet light behaves differently when subsequently exposed to light of $\lambda > 405$ nm. In the initial stages (of $\lambda > 405$ nm exposure) there is a decrease in the optical density and in figure 7 the decrease in optical density versus λ is given after exposure to 546 nm light. Similar results were obtained on exposure to 633 nm light. This bleaching effect is small compared to the increases in optical density during irradiation. On prolonged exposure to light of $\lambda > 405$ nm after ultraviolet exposure the optical density increases as it does for a sample not previously exposed.

Gas evolution (N_2) has also been observed due to exposure to this longer wavelength radiation, but the efficiency as a function of λ and previous exposure has not been investigated (ref. 5). In addition, photoconductivity has been observed throughout the wavelength range under consideration (ref. 15). The photocurrent increases continuously from long wavelength (~ 1000 nm) to the band edge.

The Δ O.D. produced by optical bleaching (fig. 7) has a distinctly different wavelength dependence than the Δ O.D. produced by irradiation and/or exposure to air or by thermal treatment. This indicates a defect distinct from the colloidal Pb (which is apparently the dominant type of disorder). The band of figure 7 resembles the F' band observed in the alkali halides (ref. 16), and since the F' band is due to weakly bound electrons the data of figure 7 suggest the presence of weakly bound electrons or holes in $Pb(N_3)_2$. However, the long wavelength radiation also produced colloidal disorder. Thus, it is necessary to consider the possibility that the band of figure 7 is the net effect of bleaching of an F' type band and growth of colloidal Pb (see figure 8 for a typical increase of O.D. versus wavelength for colloidal Pb formation). In this case, the true maximum of the band which is bleached occurs at a shorter wavelength. It is important to note that the prior ultraviolet exposure, which is a prerequisite to the optical bleaching, is absorbed in a thin surface layer ($\sim 10^4$ cm) of the crystal while the total thickness of the sample is exposed to the weakly absorbed bleaching radiation ($\lambda > 405$ nm). Thus, in the case of figure 7 the 546 nm radiation may bleach defects in the surface layer exposed to ultraviolet but generate colloidal Pb throughout the volume of the sample. Additional experiments are necessary to clarify this optical bleaching phenomenon and to understand in general the effect of long wavelength light ($\lambda > 405$ nm).

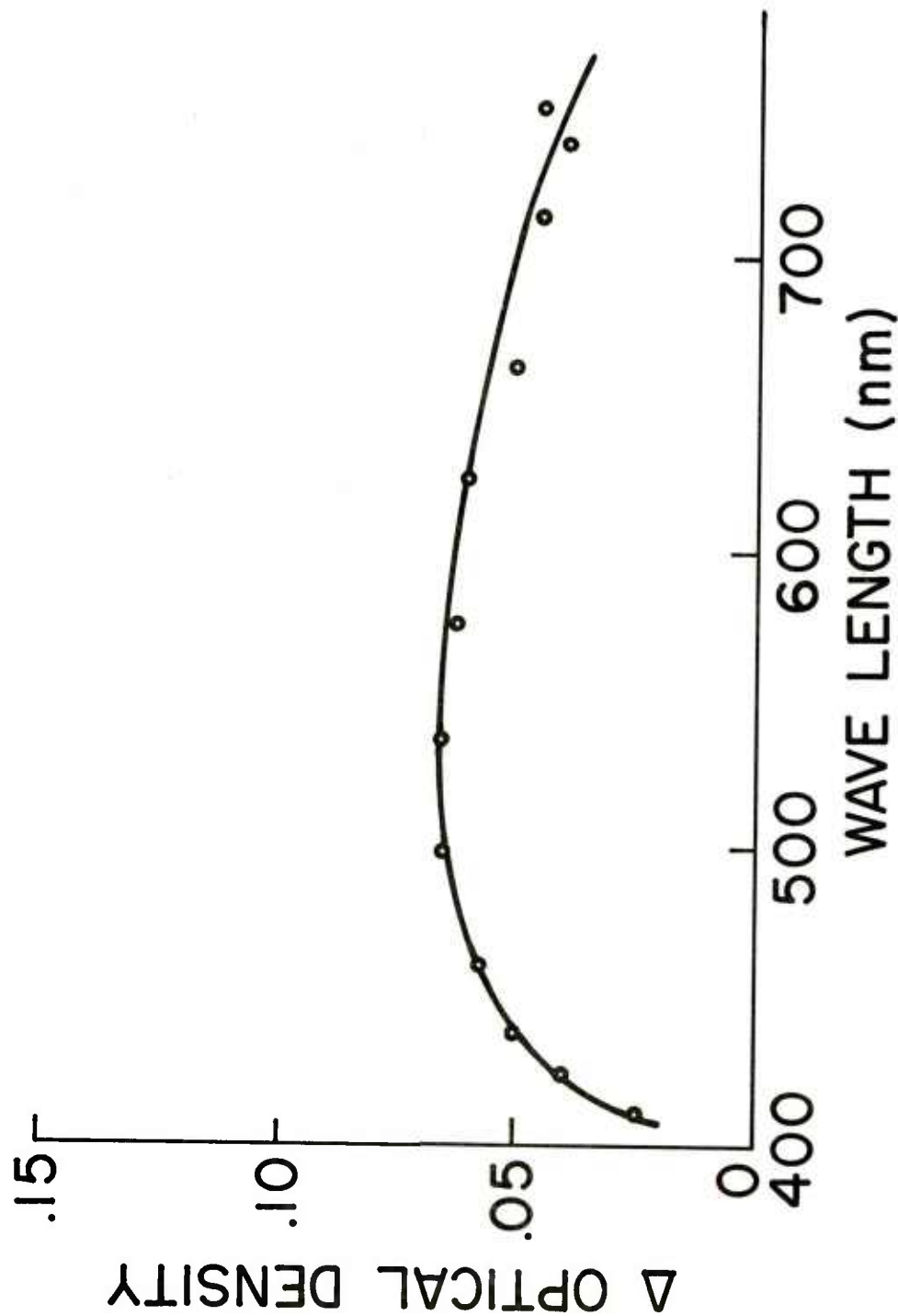


Figure 7. Decrease in optical density versus wavelength due to exposure to 546 nm radiation. Sample previously UV-irradiated. All irradiation and measurements at room temperature in the vacuum cryostat.

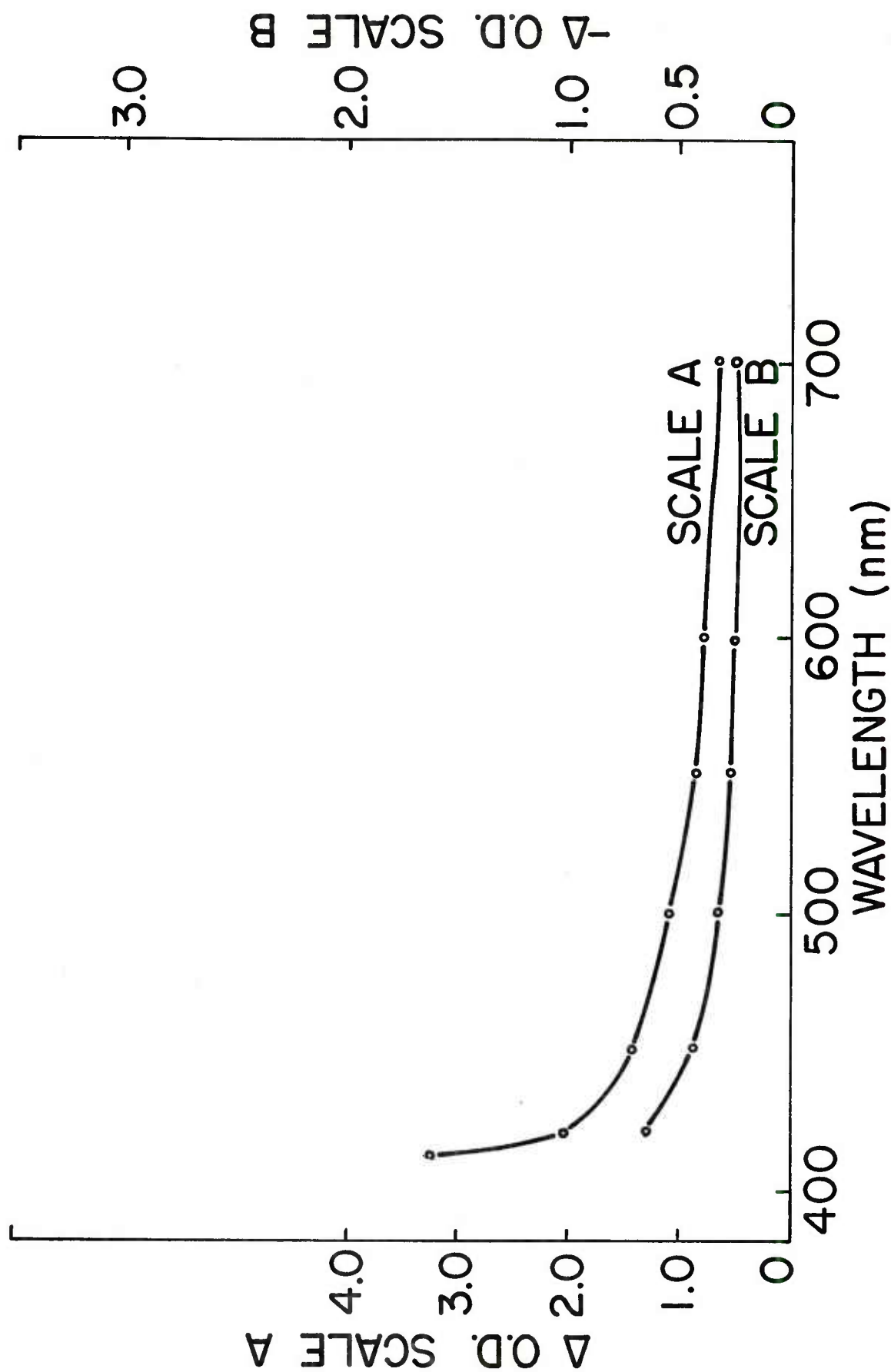


Figure 8. Decrease in optical density versus wavelength, λ , due to exposure to air of a sample previously UV irradiated in high vacuum, Scale B. Also shown is the curve of increase of optical density versus λ due to UV irradiation with sample in high vacuum, Scale A.

Colloidal Lead and Lead Metal Production

In most cases, the change in optical density (Δ O.D.) due to irradiation is typical of that to be expected of lead colloids i.e., a continuously decreasing Δ O.D. with increasing wavelength, (see fig. 8, scale A). The Δ O.D. decreases with increasing wavelength as is expected for colloids, but does become insensitive at longer wavelengths. This supports the hypothesis of a metallic lead film coexisting with lead colloids: thin lead metal films have optical density versus wavelength curves which are essentially independent of wavelength in the visible range (refs. 13, 31).

On admitting air to the system, the initial reaction may then be with the lead metal. Evidence for this is shown in figure 8 (Scale B) which gives the Δ O.D. due to reaction with air. The Δ O.D. is rather wavelength-independent thus suggesting that a significant part of it is due to loss of lead metal. There is also evidence of some loss of lead colloids.

It is to be noted that the Δ O.D. as a function of time (figs. 2,3) and total N_2 evolved (fig. 5) were taken at short wavelengths close to the band edge where the major contribution to the Δ O.D. is due to colloids. The optical extinction of a thin metallic film containing a given number of Pb atoms per unit area is expected to be different from the same area density of Pb atoms in the form of colloids. This is evident from the strong dependence of the colloidal extinction on the index of refraction of the medium surrounding the colloids (ref. 8). Some of the deviations from the expected linear relationship between Δ O.D. and total N_2 evolved may be due to the presence of the metallic Pb film (fig. 5). Other reasons for the deviation from linearity are discussed elsewhere.

We could not determine the relative amount of metallic Pb and colloidal Pb because the Pb particles may be surrounded by material of varying indices of refraction, e.g., vacuum, crystalline Pb (N_3)₂ of various orientations and indices of refraction, or compounds formed during or after irradiations. The data for some samples irradiated in the high vacuum system do not indicate the presence of metallic Pb. At this time the conditions which lead to the formation of metallic Pb have not been determined. Irradiation dose, surface morphology, perfection and contamination of the unirradiated sample are among factors which may be important.

There is some evidence for a thinner Pb metal film produced by irradiation of samples mounted in the cryostat. Many of the Δ O.D. versus λ curves obtained in this way do show a flattening of the curve,

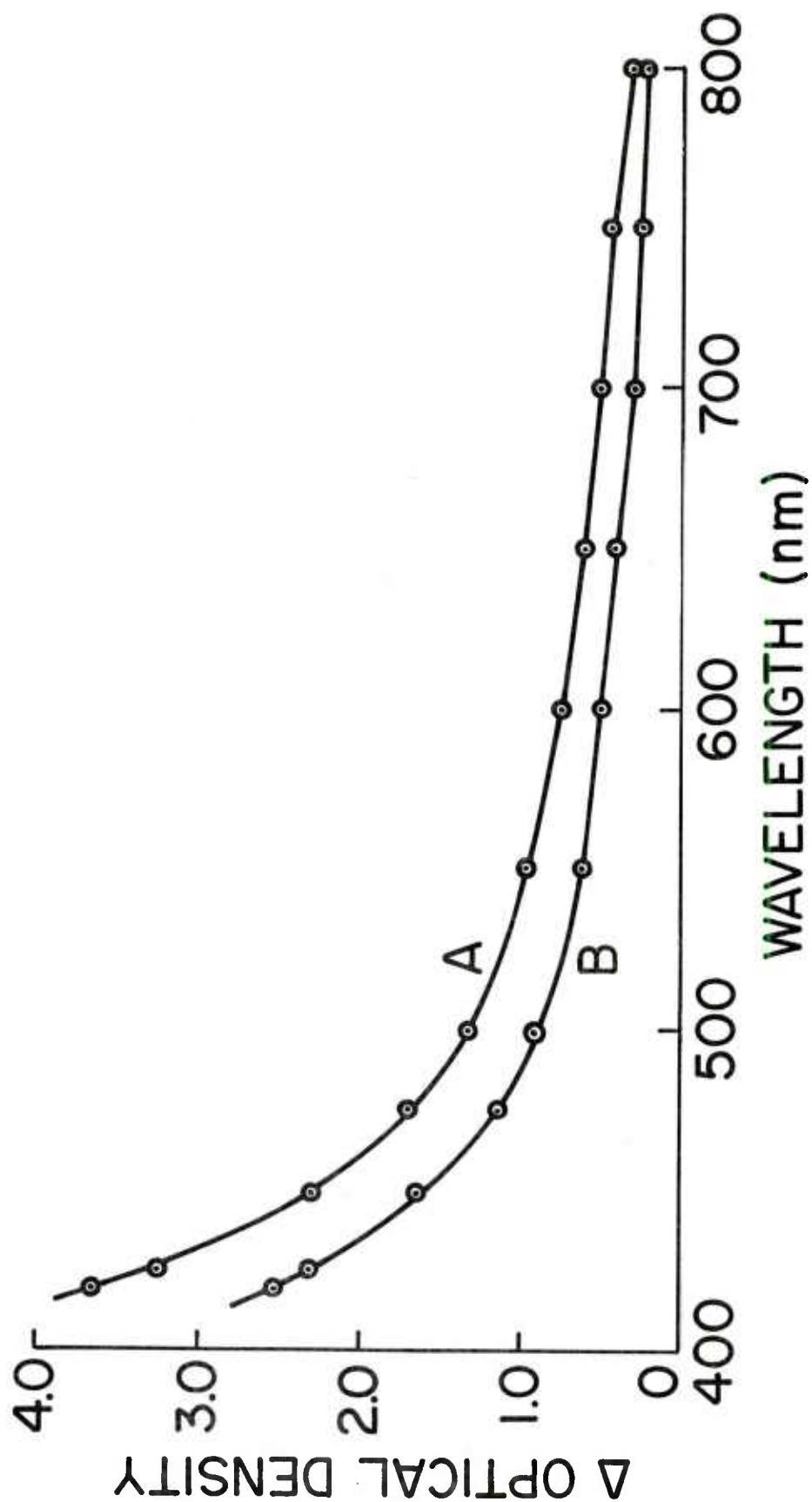


Figure 9. Increase in optical density versus λ due to irradiation with 435.6 nm light. Data is given for the electric field, \bar{E} , parallel to the \bar{b} (Curve A) and \bar{c} (Curve B) crystallographic directions.

i.e., λ independence at longer wavelengths, although the Δ O.D.'s are small and may be close to the experimental uncertainty. (The latter is determined by the ability to reproduce the sample - cryostat position in the Cary beam since the samples are not damaged uniformly (ref. 8). However, one sample which was heavily UV irradiated at 80K gave a Δ O.D. versus λ curve which decreased continuously with increasing wavelength to 1600 nm, thus giving no evidence of Pb metal for these conditions. Additional experiments are necessary to resolve this matter.

A significant metallic lead film may not have formed in the cryostat because the pressure was sufficiently high to allow reactions to occur during irradiation. Thus, the surface colloidal lead particles were, for the most part, coated with at least a thin nonconducting layer and a significant continuous metal film did not form. Because of the possibility of chemical reactions, it is also possible that compounds e.g., Pb oxides and Pb nitrogen compounds contribute to the changes in optical density due to irradiations. But it is clear that most of the Δ O.D. is due to Pb colloids with some contribution from Pb metal.

Index of Refraction Measurements

The calculations of the extinction to be expected for colloidal Pb particles embedded in $\text{Pb}(\text{N}_3)_2$ were made assuming that the index of refraction, n , is independent of wavelength (ref. 8). This was a necessary approximation because the λ dependence of n was unknown. While it is to be expected that n is a weak function of λ over at least most of the λ range of interest (because of the absence of absorption in unirradiated $\text{Pb}(\text{N}_3)_2$), a λ dependence of n has been reported for AgN_3 (ref. 17). The magnitude of the colloidal extinction is very sensitive to the magnitude of n : an increase of n from 1.0 to 2.0 results in approximately a calculated tenfold increase in extinction (refs. 8,18). Thus, even small changes in the index as a function of λ may strongly affect the observed λ dependence of the extinction. In addition, for $\text{Pb}(\text{N}_3)_2$ a highly anisotropic index has been reported (ref. 19). Thus, the colloidal extinction will depend on crystal orientation. In order to remove any uncertainty concerning this question, measurements were made of n as a function of λ and crystal orientation.

The index, n , was determined using a Zeiss polarizing microscope to determine the apparent and actual thickness of polished $\text{Pb}(\text{N}_3)_2$ single crystal plates. A high pressure Xe 1000 watt lamp and either a monochromator or interference filters were used as the source of light. The single crystals were oriented by x-ray diffraction and measurements were made on two polished plates with faces containing the \bar{a} and \bar{b} and \bar{b} and \bar{c} axes respectively where the convention $\bar{a} = 11.31$, $\bar{b} = 16.25$, $\bar{c} = 6.63$ Å is used.

The values at 528 nm are $n_c = 1.85$, $n_a = 2.20$, $n_b = 2.55$ and are in agreement with the values reported by Hattori and McCrone (ref. 19). In addition, all three values were found to be independent of λ between 450 and 650 nm. The wavelength range was limited by the sensitivity of the eye in focusing the microscope.

These results justify the use of an n independent of λ in the calculations of colloidal Pb extinction in $\text{Pb}(\text{N}_3)_2$ (ref. 8). The λ -dependence of n as reported for AgN_3 (ref. 17) may be due to decomposition and the resulting absorption due to imperfections. The extinction due to Pb colloids in $\text{Pb}(\text{N}_3)_2$ will, however, depend on the crystal orientation and polarization of the measuring light beam.

Optical Extinction Studies Using Polarized Light

For these studies, plate-shaped crystals of lead azide were used. Bulk crystals were oriented by back reflection Laue photographs before cutting, and the resulting plates checked by the same technique were nominally aligned to within 3° . Crystal plates having \bar{a} , \bar{b} , and \bar{c} perpendicular to the plane of the plate were measured in transmission using the Cary 14R Spectrophotometer. Polarizing sheets were placed in both the sample and reference beams of the Cary with \bar{E} parallel to \bar{a} , \bar{b} , and \bar{c} .

Three unirradiated samples with the orthorhombic axes \bar{a} , \bar{b} , and \bar{c} , respectively, normal to the plane of the plate were measured. The optical density versus wavelength curves indicate a sharp rise in extinction with decreasing wavelength at about 400 nm. The rise is the same for \bar{E} parallel to \bar{a} and \bar{c} within experimental error. However, the extinction (absorption) "edge" is shifted by approximately 4 nm or 0.03 eV. to the red for \bar{E} parallel to \bar{b} . From the structure of $\text{Pb}(\text{N}_3)_2$ (ref. 20), it can be seen that of the 24 azide molecules in the unit cell, 12 of these are aligned nearly in the \bar{b} direction. These results indicate that the azide ions as influenced by the crystal field is associated with the absorption process at the edge at 400 nm. Unfortunately, the measurements could not be extended to observe the peak at 375 nm (ref. 13) because of the high extinction coefficients. However, these results do indicate the need to investigate the polarization dependence of the reflectivity or the absorption of single crystal thin films at shorter wavelengths. These may help to elucidate the type of electronic transition responsible for the structure at 375 nm, give insight into the type of excitons produced by absorption of light, and determine if the peak at 375 nm is associated with one of the four non-equivalent azide ion sites as suggested (refs. 6,21). It would also be interesting to make photoconductivity studies as a function of light polarization. Available results indicate a relationship between the 375 nm peak and structure in the photoconductive response versus wavelength

(ref. 15). Finally, photodecomposition studies as a function of electric field vector orientation may help elucidate the mechanisms of photodecomposition (ref. 22).

Studies have also been made of the polarization dependence of irradiation induced extinction. For colloidal extinction a dependence on the index of refraction, n , of the surrounding medium is predicted (refs. 8, 18). For $\text{Pb}(\text{N}_3)_2$ the irradiation induced extinction should then depend on the orientation of \vec{E} relative to the crystallographic axis because of the dependence of n on orientation if in fact the extinction is due to colloids. In addition, it should be possible to distinguish between scattering and absorption due to colloids because of the dependence on n .

Measurements were made on one single crystal plate having the \vec{b} and \vec{c} axis lying in the plane of the plate. These axes were chosen to maximize any differences dependent on n . Two wavelengths of damaging radiation were used. The output of a high pressure Hg lamp was passed through a water filter and a 436.0 or a 365.0 nm interference filter. The 436.0 nm irradiation is only very weakly absorbed in unirradiated material (ref. 8) whereas the 365.0 nm radiation is strongly absorbed (refs. 6, 13) and produces damage only in a thin surface layer ($\sim 10^5$). The latter has been verified by polishing after irradiation, which removed the irradiation-induced coloration. The damage distribution for 436.0 radiation is discussed below. The increase in O.D. due to the 436 nm irradiation is shown in figure 9 where Curve B is obtained for \vec{E} parallel to \vec{c} and Curve A for \vec{E} parallel to \vec{b} . The ratio of the change in O.D., i.e.,

$$R = \frac{\Delta \text{O.D.}(\vec{E} \parallel \vec{b})}{\Delta \text{O.D.}(\vec{E} \parallel \vec{c})} ,$$

has a value of about 1.5 and is independent of wavelength within the precision of the measurements. Our calculations (based on ref. 18) predict a value of $R \approx 2.2$ for absorption and $R \approx 4.0$ for scattering, both values being insensitive to wavelength. Thus, the experimental value of 1.5 for R suggests that the $\Delta \text{O.D.}$ is due primarily to colloidal absorption.

Experimental and theoretical factors affecting R must be considered in placing rough limits on the accuracy and precision of this quantity. The agreement between experiment and theory is good considering the assumption of colloids as isolated, spherical, non-interfering, scattering, and absorbing particles, having bulk Pb metal optical properties. In addition, experimental conditions tend to yield a value of R that is smaller than the actual value: surface scratches on the crystal faces tend to depolarize the beam, effectively lowering the value of R . A lower value of R was obtained when the measuring beam was incident on a surface having microscopically observable scratches. Also, the alignment of the polarizing sheets with respect to the crystallographic axes was in error by a few degrees due to errors in maintaining crystallographic alignment during cutting and polishing. Thus, more exacting results could be obtained through the use of better surface polishing, and precise alignment fixtures. Hence, due to these experimental uncertainties, scattering or a combination of scattering and absorption can not be completely ruled out.

Polarization dependent extinction due to UV irradiation (primarily 365 nm) was also studied. In this case, no differences were found for light polarized parallel to \bar{b} or \bar{c} : both gave the same Δ O.D. versus λ curve. This result is attributed to the fact that the 365 nm radiation is absorbed in a thin surface layer, thus producing sufficient disorder so that the index becomes independent of polarization. This conclusion is supported by quantitative measurements of N_2 evolution in the high vacuum system and knowledge of the absorption coefficient of the damaging radiation. If it is assumed that the damage (decomposition) decreases exponentially with distance from the irradiated surface, as does the absorption coefficient, then decomposition at this surface is estimated to be greater than 50%. The results are also in agreement with x-ray photoelectron spectroscopy studies which show that essentially all of the nitrogen is removed from very thin (10-50 Å) surface layers (ref. 23).

In order to differentiate between bulk and surface photodecomposition, a $Pb(N_3)_2$ crystal was exposed to both the 436 nm and 365 nm irradiation, and then removed from the cryostat and polished briefly on both surfaces to remove approximately 50 μ . This treatment removed the damage caused by the UV irradiation, but left a significant Δ O.D. which is attributed to colloids in the bulk resulting from the 436 nm irradiation. A second polishing of both surfaces (50 μ removed) failed to completely remove the colloidal absorption, thus verifying that colloids were produced in the bulk.

McLaren (ref. 24) also found a lack of dependence of colloidal extinction on polarization for UV irradiated AgN_3 (ref. 24). In this material, a maximum in the curve of extinction versus wavelength is

expected, and further the wavelength at which the maximum occurs is expected to be polarization-dependent because of the non-isotropic index of refraction. The apparent wavelength for the maximum was found to be polarization-independent and McLaren interpreted his results in terms of Ag colloidal particles on the surface of AgN_3 and thus primarily surrounded by air. The wavelength of the maximum is also in better agreement with that predicted on the basis of Ag particles surrounded by air than surrounded by AgN_3 . This interpretation is open to question, however, because of the amount and distribution of Ag necessary to produce the observed extinction. For the predicted colloidal extinction to be observed, the colloidal particles must be separated by distances; large, compared to their size and the wavelength of measuring light. If these conditions are not met, the extinction might be expected to approach that of a Ag metal film, i.e., independent of wavelength in the range of measurements, and possibly to exhibit interference effects. An alternative explanation of McLaren's results is that the colloidal Ag particles were embedded in a highly disordered and porous matrix of AgN_3 having a low and isotropic value of n . It might be possible to distinguish experimentally between these two interpretations by replica electron microscopy. While direct electron microscopy and electron diffraction studies have been made, the results are thought to be complicated by thermal decomposition due to heating by the electron beam (refs. 25, 26). Polarization dependent maxima roughly as predicted by theory were found after thermal decomposition of AgN_3 by McLaren. In the case of irradiated $\text{Pb}(\text{N}_3)_2$, colloidal particles of Pb on the surface would be at least partially converted to lead compounds because only a fore vacuum was used. Exposure of the sample to atmospheric conditions did not alter the polarization results.

DISCUSSION

Structure and Surface Morphology of Irradiated Lead Azide

The results of the previous sections indicate that the structure and form of irradiated $\text{Pb}(\text{N}_3)_2$ depends on the pressure during or after exposure and possibly on the temperature during exposure. An attempt is made here to rationalize the results in terms of possible structures.

The first question to address is the location of the damaged regions relative to energy density of absorbed radiation. Williams and coworkers (ref. 7) have argued from studies of infrared absorption of thin films of uv-irradiated lead azide that the damage decreases with distance from the irradiated surface and thus occurs in the region of energy absorption. If this is the case, the density of colloidal Pb particles should decrease in this manner with distance from the surface. Thus, we might expect a sufficiently high density of Pb or

Pb particles, e.g., colloids, at the outer surface which can be completely devoid of nitrogen (see below) to form a layer of Pb having metallic properties. This may be a very porous form of Pb having an extremely high surface-to-volume ratio. At greater distances from the irradiated surface the density of absorbed energy is lower and hence the density of colloidal Pb. Thus, there may be a gradient from metallic-like Pb at the outer surface to colloidal Pb embedded in lead azide to undamaged lead azide. The density of trapped nitrogen should be quite different as a function of distance from the irradiated surface because the probability of escape should decrease with increasing distance.

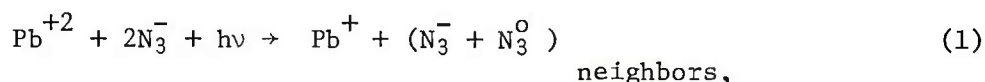
The x-ray photoelectron spectroscopy (XPS) studies have shown that $\text{Pb}(\text{N}_3)_2$ powders, which are essentially stoichiometric before irradiation, can be converted to lead or lead compounds by UV or x-ray irradiation, i.e., all nitrogen can be removed from the surface layers sampled by this technique (refs. 22, 27). The sampling, however, may comprise only a few atomic layers. The irradiations were carried out nominally at room temperature or somewhat above and at pressures of approximately 2×10^{-6} torr. These results lend support to the interpretation of the optical data in terms of a small amount of metallic-like Pb being produced by irradiation of single crystal samples in the high vacuum system. While there is some evidence of oxide formation from the XPS studies, compound formation is difficult to substantiate because there is always significant oxygen and carbon contamination on the surface of almost all materials studied, including the azides. In other cases, XPS studies revealed the presence of a new form of nitrogen, possibly in the form of a nitride, after complete removal of the azide nitrogen. Complete decomposition by x-ray irradiation in air has been found by x-ray diffraction to result in basic lead carbonate (ref. 28). So the outer surface of irradiated lead azide may have a layer of metallic Pb and/or Pb compounds with carbon and oxygen contamination. It may also be significant to point out that the surface of unirradiated lead azide decomposes slowly in air with loss of nitrogen. Apparently, however, a protective surface layer is formed which prevents or significantly retards decomposition because grinding to produce fresh surface reveals material with a much higher azide nitrogen content than that of old surface (ref. 27).

The outer surface layers of lead azide irradiated in high vacuum may then be made up of highly porous Pb metal and colloidal particles partially embedded in $\text{Pb}(\text{N}_3)_2$. Thin layers of carbon and oxygen are also present either by adsorption or in the form of compounds. The high reactivity of this Pb is attributed to a high surface-to-volume ratio. The reaction may also be catalyzed by compounds formed during irradiation. Lead particles (colloids) may also occur along dislocations

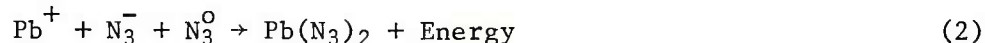
in $\text{Pb}(\text{N}_3)_2$ and may react with air by air diffusing into the material in the same way as the nitrogen escapes, e.g., along dislocations. Ag metal is known to precipitate along dislocations in irradiated silver halides (ref. 29). As already discussed, McLaren attributed the optical extinction of irradiated AgN_3 to silver particles on the surface of AgN_3 being surrounded by air and not AgN_3 (ref. 30).

Decomposition Model

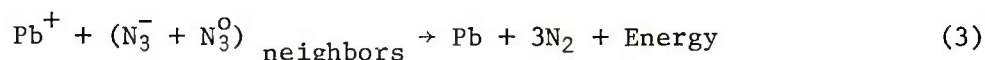
We propose a model to explain the observed kinetic behavior of the nitrogen evolution and the formation of lead colloids. The primary absorption process leading to decomposition is assumed to involve the transition of an electron from an azide ion to a lead atom, an azide ion excited state, or a conduction band electron. The rate of evolution of N_2 is assumed to be proportional to that of N_2 creation (rapid diffusion), and likewise that the diffusion of lead is not a rate limiting step in the formation of lead colloids. The proposed reaction scheme can be expressed as follows:



where the products from Reaction 1 can react to give either a reversion to the initial state:



or a decomposition reaction:



Reaction 1 represents one possible excitation process of those mentioned previously that could lead to decomposition. In order to explain the observed first order kinetics it is assumed, in Reaction 3, that a neutral azide molecule reacts with a neighboring unexcited molecule.

The kinetic equations for these three reactions (with low irradiation levels) are given as follows:

$$\frac{d [\text{N}_3^-]}{dt} = -a[\text{N}_3^-] + b[\text{N}_3^0] \quad (4)$$

$$\frac{d [\text{N}_3^0]}{dt} = a [\text{N}_3^-] - b[\text{N}_3^0] - c [\text{N}_3^0] \quad (5)$$

$$\frac{d [3/2N_2]}{dt} = c [N_3^0] \quad (6)$$

where $[N_3^-]$, $[N_3^0]$, and $[3/2N_2]$ are the concentrations, b and c are rate constants, and $a = g\alpha I_0 e^{-\alpha x}$ where g is a constant, α is the absorption coefficient and x , the distance into the sample. The simultaneous solution of the rate equations for the boundary condition that at $t = 0$, $[N_3^-] = [N_3^-]_0$ and $[N_3^0] = [N_2] = 0$, yields for the concentration of nitrogen and lead produced at time t for an energy deposition rate of a :

$$[Pb] = 3[N_2] = \frac{2ca[N_3^-]_0}{r_2 - r_1} \left[\left(\frac{1-e^{r_1 t}}{r_1} \right) - \left(\frac{1-e^{r_2 t}}{r_2} \right) \right] \quad (7)$$

where both r_1 and r_2 are negative and equal to:

$$r_{1,2} = \frac{-(a + b + c) \pm \sqrt{(a + b + c)^2 - 4ac}}{2} \quad (8)$$

and $|r_2| > |r_1|$. Equation 7 can be simplified by making certain approximations concerning the magnitude of the rate constants and the energy deposition rate. Since the quantum efficiency for the production of nitrogen or lead is low, it will be assumed that $b \gg c$, namely, that an excited azide ion has a much greater probability of returning to the ground state than of reacting to form nitrogen. In addition, quantitative arguments indicate that for the intensities used in these experiments, the condition that $b \gg a$ also holds. With these approximations, the expressions for r_1 and r_2 reduce to:

$$r_1 \approx -\frac{ac}{b} \quad \text{and} \quad r_2 \approx -b \quad (9)$$

Substituting these values of r into equation 7 gives the time dependence for the production of lead or nitrogen:

$$[Pb] = 3[N_2] \approx 2ac [N_3^-]_0 \left[\frac{(1-e^{-\frac{ac}{b}t})}{ac} - \frac{(1-e^{-bt})}{b^2} \right] \quad (10)$$

and the nitrogen evolution rate is found simply by differentiating equation 10:

$$\frac{d[N_2]}{dt} = \frac{2ac}{3b} [N_3^-]_o [e^{-\frac{ac}{b}t} - e^{-bt}] \quad (11)$$

Equations 10 and 11 are valid for any laminar region a distance x from the surface where the light intensity is given by $I = I_o e^{-\alpha x}$ and the rate constant a , by $a = g\alpha I$. Thus, the total amount of lead produced or the total rate of nitrogen evolution can be obtained by integrating equations 10 and 11 over the exposed sample volume.

The integral of equation 11 is given as follows:

$$\frac{d[N_2]}{dt} = \frac{2Ac[N_3^-]_o}{3b} \int_0^{\ell} g\alpha I_o e^{-\alpha x} [e^{-\frac{g\alpha c I_o t}{b} e^{-\alpha x}} - e^{-bt}] dx \quad (12)$$

where A is the exposed surface area, ℓ is the sample thickness and one dimensional geometry is assumed, so that $dV = Adx$. Integration of equation 12 in the limit $\ell \rightarrow \infty$ which is valid for uv exposures where $\ell \gg 1/\alpha$, yields:

$$\frac{d[N_2]}{dt} = \frac{2A}{3} [N_3^-]_o \left[\frac{1 - e^{-g\alpha I_o \frac{c}{b} t}}{\alpha t} - \frac{c}{b} g I_o e^{-bt} \right] \quad (13)$$

equation 13 does not represent the total measured nitrogen evolution rate as some nitrogen will still be lost by diffusion into the lattice and subsequent trapping. This expression is similar to the rate equation derived from a simpler decomposition model by Williams et al., for thin films (ref. 9).

The growth of the lead concentration with time is found by integrating equation 10 over the exposed volume, which in the limit $\ell \rightarrow \infty$ yields:

$$[Pb] \approx \frac{2[N_3^-]_o}{\alpha} \left[\left(\frac{\alpha I_o c}{b} \right) t - \left(\frac{\alpha I_o c}{b} \right)^2 \frac{t^2}{2.2!} + \left(\frac{\alpha I_o c}{b} \right)^3 \frac{t^3}{3.3!} - \dots - \frac{\alpha I_o c}{b} (1 - e^{-bt}) \right] \quad (14)$$

The expressions for the total rate of nitrogen release and the total lead produced can now be compared to the experimental results of nitrogen evolution rates and changes in optical density. Because the integration of equations 10 and 11 over volume does not change the qualitative features of the results, we will confine the discussion to the mathematically simpler expressions given by equations 10 and 11.

The total lead produced as given in equation 10 can be further simplified by using the approximation $b \gg \frac{ac}{b}$ to give:

$$[Pb] \approx 2[N_3^-]_0 \left(1 - e^{-\frac{ac}{b} t}\right) \quad (15)$$

This result is in qualitative agreement with the saturation curves observed experimentally (fig. 2) and thus lends support to the assumptions made concerning the magnitude of the rate constants. For the case where $t \gg b/ac$, equation 15 can be expanded to give:

$$[Pb] = 3[N_2] \approx 2[N_3^-]_0 \frac{c}{b} \alpha I t \quad (16)$$

which shows a linear increase with both time and light intensity as is observed experimentally for small amounts of decomposition (figs. 2,3), and for exposures at low light intensity (fig. 4).

The nitrogen evolution rate given in equation 11 can also be further simplified. Because $b \gg \frac{ac}{b}$, this equation predicts a rapid rise to approximately $\frac{dN_2}{dt} = \frac{2ac}{3b} [N_3^-]_0$, and for $t \gg b$ reduces to:

$$\frac{d[N_2]}{dt} = \frac{2ac}{3b} [N_3^-]_0 e^{-\frac{ac}{b} t} \quad (17)$$

The rapid rise is too fast to be followed by the instrumentation and thus, figure 1 indicates a finite $\frac{dN_2}{dt}$ at $t = 0$. Thus, following the

induction period, the kinetic results are also in qualitative agreement with the rate calculated in equation 17. The rate decays approximately exponentially with a time constant that decreases for increasing intensity as shown in figure 1 for the 365 nm irradiation. Thus, with the proposed model, it is possible to explain at least the qualitative features of the gas evolution rates and the changes in O.D. and their dependence on intensity and time. Diffusion effects are also clearly present in

the formation of lead colloids and the escape of nitrogen gas but they do not appear to influence the decomposition rates with the exception of the induction period and the dependence on temperature and wavelength. The efficiency curve (fig. 6) indicates that the nitrogen evolution rate and the absorption coefficient have a similar dependence on wavelength. As all the energy in the beam is being absorbed by the sample, this dependence of gas evolution rate on wavelength must be a consequence of the rate at which nitrogen arrives at the surface. For more strongly absorbed light, the decomposition occurs closer to the surface and, consequently, less nitrogen is lost through diffusion into the sample. It can be assumed from the observation on gas trapping during the induction period that N_2 which diffuses into the lattice can be trapped there and so not contribute to the observed rate. Lead atoms may be formed directly during the decomposition Reaction 3, and diffuse to form colloids, or Pb^+ plus electrons may diffuse independently to form colloidal lead as in the silver halides.

REFERENCES

1. J.M. Groocock, "The Decomposition of α -Lead Azide", Proceedings of 2nd Detonation Symp., 1, 411 (1955).
2. V.R. Pai Verneker, A.C. Forsyth, "Photodecomposition of α -Lead Azide in the Solid State", J. Phys. Chem. 71, 3736 (1967).
3. W.L. Garrett, "Crystal Growth and Photodecomposition of Lead Azide", Ph.D. Thesis, U. of Delaware (1972).
4. Yu. A. Zakharov, S.M. Ryabykh, A.P. Lysykh, "X-Ray Induced Decomposition of Single Crystals of PbN_6 ", Kinetika i Kataliz, 9, 679 (1968).
5. Yu. A. Zakharov, Ye. P. Abakumov, E.P. Surovoy, Izv. Tomsk. "Photolysis of Azides of Lead, Silver, and Certain Systems Based on Them", Politekh Inst., 251, 373 (1970).
6. R.B. Hall, F.E. Williams, "Photodecomposition and Electronic Structure of Lead Azide", J. Chem. Phys., 60, 4950 (1974).
7. S.P. Varma, F. Williams, K.D. Moller, "Effect of Photodecomposition on the Infrared Spectra of Lead Azide. I. For Infrared", J. Chem. Phys. 60, 4955 (1974).
8. D.A. Wiegand, "Photoproduction of Disorder in $Pb(N_3)_2$ and TiN_3 ", Phys. Rev. B, 10, 1241 (1974) and Picatinny Arsenal Technical Report 4080, Dover, NJ 07801 (1970).
9. S.P. Varma, F.E. Williams, "Effect of Photodecomposition on the Infrared Spectra of Lead Azide. II. Near Infrared", J. Chem. Phys., 60, 4955 (1974).
10. G.G. Savelyev, Yr. V. Gavrishchenko, V.L. Shcherinskiy, S.I. Rukoleyev Izv. Tomsk. Politekh Inst. "Mechanism of Lead Azide Photolysis", 199, 116 (1969).
11. D.A. Young, Vol. 5 Progress in Solid State Chemistry, H. Reiss, Ed. Pergamon Press, 1970.
12. W.L. Garrett, "The Growth of Large Lead Azide Crystals", Mat. Res. Bull. 7, 949 (1972).
13. H.D. Fair, Jr., A.C. Forsyth, "Optical and Electrical Properties of Thin Films of α -Lead Azide", J. Phys. Chem. Solids 30, 2559 (1969).

14. R.B. Hall, "Studies of Electronic Structure and Chemical Instability in Lead Azide", Ph.D. Thesis, U. of Delaware (1972).
15. W.H. Taylor, II, M. Blais, "Photoconductivity in Crystals and Thin Films of α -Lead Azide", Bull. Am. Phys. Soc., March 1968 and H.D. Fair, Jr., A.C. Forsyth, "Thin Film and Single Crystal Investigations on Transition Metal-Doped Lead Azide", Proceedings of the 6th International Symposium on the Reactivity of Solids, Eds. J.W. Mitchell, B.C. DeVries, R.W. Roberts, P. Cannon, John Wiley and Sons, New York (1969).
16. J.H. Schulman and W.D. Compton, Color Centers in Solids, MacMillan Co., New York (1962), 108.
17. A.D. Yoffe, "The Inorganic Azides", Developments in Inorganic Nitrogen Chemistry, E.C.B. Colburn, Ed., Elsevier, Amsterdam (1966).
18. H.C. Van de Holst, Light Scattering by Small Particles, John Wiley and Sons, New York (1957).
19. K. Hattori and W. McCrone, "Lead Azide, $Pb(N_3)_2$ ", Anl. Chem. 28, 1791 (1956).
20. C.S. Choi, E. Prince, and W.L. Garrett, "Refinement of α -Lead Azide by Neutron Diffraction", Acta Cryst., B33, 3536 (1977).
21. S.P. Varma and F.E. Williams, "Infrared Absorption Spectra of Doped and Undoped Lead Azide", J. Chem. Phys. 59, 912 (1973).
22. F. Owens, "Evidence for the Role of Excitons in the Production of Paramagnetic Defects in the Azides", Phys. Rev. 2B, 2064 (1970).
23. J. Sharma, P. Plaksin, S. Bulusu, and D. Wiegand, "X-Ray Photoelectron Spectroscopy Applied to the Study of Radiation Damage", Am. Chem. Soc. Meeting, Rochester, NY, Oct. 1973.
24. A.C. McLaren, "The Absorption Spectra of Single Crystals of Pure and Partially Decomposed Silver Azide", Proc. Phys. Soc. B70, 147 (1957).
25. J. Sawkill, "Nucleation in Silver Azide: An Investigation by Electron Microscopy and Diffraction", Proc. Roy. Soc. A229, 135 (1955).
26. F.P. Bowden and A.D. Yoffe, Fast Reactions in Solids, Academic Press, New York (1958).

27. D.A. Wiegand, J. Sharma, "X-Ray Photoelectron Spectroscopy (XPS) Studies of Irradiation Induced Decomposition of Heavy Metal Azides and Other Materials", Bull. Am. Phys. Soc. 19, 283 (1974) and unpublished results.
28. G. Todd and E. Parry, "Radiation-Induced Changes in Alpha-Lead Azide", Nature 186, 543 (1960).
29. J.M. Hedges and J.W. Mitchell, "Some Experiments on Photographic Sensitivity", Phil. Mag. (7) 44, 357 (1953).
30. A.C. McLaren, "The Absorption Spectra of Single Crystals of Pure and Partially Decomposed Silver Azide", Proc. Phys. Soc. B70, 147 (1957).
31. R.B. Hall, "Studies of Electronic Structure and Chemical Instability in Lead Azide", Ph.D. Thesis, University of Delaware (1972).

DISTRIBUTION LIST

Defense Documentation Center (12)
Cameron Station
Alexandria, VA 22314

Department of Defense
Explosive Safety Board
Washington, DC 20314

Commander
US Army Armament Material Readiness Command
ATTN: DRSAR-LC
Rock Island, IL 61201

Commander
US Armament Research and Development Command
ATTN: DRDAR-LCU-E (2)
DRDAR-LCM (5)
DRDAR-LCE (25) Dr. W. Garrett
DRDAR-QA
DRDAR-TSS (5)
Dover, NJ 07801

Director
Ballistic Research Laboratory
USA, ARRADCOM
ATTN: DRDAR-TB
Aberdeen Proving Ground, MD 21005

Commander
Naval Surface Weapons Center
White Oak Laboratory
ATTN: Technical Library
Silver Spring, MD 20910

Commander
Air Force Armament Development and Test Center
ATTN: AFB Technical Library
Eglin Air Force Base, FL 32542

Lawrence Livermore Laboratory
ATTN: Technical Library
P.O. Box 808
Livermore, CA 94550

Los Alamos Scientific Laboratory
ATTN: Technical Library
Mr. T. Benzinger
Los Alamos, NM 87544

J.C. Brower Associates, Inc.
2040 N. Towne Ave.,
Pomona, CA 91767

Commander
US Army Armament Materiel Readiness Command
ATTN: DRSAR-LEP-L
Rock Island, IL 61299

Director
US Army TRADOC Systems Analysis Activity
ATTN: ATAA-SL (Tech Library)
White Sands Missile Range, NM 88002

Weapon System Concept Team/CSL
ATTN: DRDAR-ACW
Aberdeen Proving Ground, MD 21010

Technical Library
ATTN: DRDAR-TSB-S
Aberdeen Proving Ground, MD 21005

Technical Library
ATTN: DRDAR-CLJ-L
Aberdeen Proving Ground, MD 21010

Benet Weapons Laboratory
Technical Library
ATTN: DRDAR-LCB-TL
Watervliet, NY 12189

US Army Materiel Systems Analysis Activity
ATTN: DRXSY-MP
Aberdeen Proving Ground, MD 21005

Ch, Demolition Branch
Special Forces School
USIMA
ATTN: Staff Sgt. Monahan
Ft. Bragg, NC 28307